TMS016 Project 3 - Final report
Iris recognition

Jack Sandberg
Sara Arnesen
David Nordström

May 2022

Abstract

This report explores methodologies used for iris recognition using 460 images provided in the MMU Iris dataset. The methodology used is an alteration of the procedure proposed in 2004 by John Daugman in his classic work 'How Iris Recognition Works' [1]. The most important tools include pre-processing, using a Gaussian filter, iris segmentation, using Daugman's integro-differential operator, feature extraction, using 2D Gabor wavelets with 1024 bits encoding, and pattern matching, using Hamming distances. The procedure used deviates from Daugman's by applying fewer Gabor filters for encoding and using the Hamming distance, instead of the fractional Hamming distance.

The findings show that the integro-differential operator accurately identifies the inner and outer boundaries of the iris in the majority (77.27%) of the instances. For the individuals where the iris boundaries were deemed good, our we achieve a 95.8% accuracy in pattern matching when comparing all samples from an individual. When restricting the comparison against one sample per individual, we obtain an accuracy of 77.7%.

1 Introduction

Recognizing individuals in an automatic- and reliable way has been an objective for a long period [1][2]. The key issue for most image-recognition problems is the relation between inter-class and intra-class variability. Objects can be reliably classified only if the variability among different instances of a given class is less than the variability between classes [1]. This poses a great challenge, especially when using face recognition as different faces possess the same basic set of features in the same canonical geometry. However, there is a mathematical advantage when utilizing the iris, as it has great pattern variability between people [1]. Another advantage is that the iris is a protected internal organ and thus very stable throughout a lifespan. Furthermore, its random texture is complex and unique, enabling recognition decisions with sufficiently high confidence levels.

There are several applications where iris recognition is used today, such as automated border crossing (instead of using passports), controlling access to restricted areas, or database access to mention a few [1][2].

The purpose is to explore methodologies used for iris recognition algorithms, by following the

research made by John Daugman. The focus will be on understanding the methods and attempting to create an iris recognition algorithm that can accurately classify eye images.

There will be no comparison in the implementation between different methodologies, such as Daugman's integro-differential operator or Hough transformation, as Daugman's method has seen global adoption and extensive commercial use the project focuses on the intricacies of his proposed method. However, for the theoretical aspects of the project, various methods will be highlighted.

The project scope will be limited to iris delineation from eye images, feature extraction based on wavelet methods, and using Hamming distance for pattern matching. Iris recognition is one of the most effective ways of identifying a person. Hence, this project serves as the first step toward a full-scale iris recognition algorithm.

2 Related work

2.1 A brief history

The concept of using iris patterns as a mean to identify a individual was proposed by Frank Burch in 1936 [3]. Leonard Flom and Aran Safir made an extensive study of the claim and proposed the concept that no two iris are alike. In 1987 they were awarded a patent [3][4]. A practical or commercial iris recognition algorithm wasn't developed until 1989. The researcher behind the algorithm was John Daugman [3][4].

2.2 Daugman's algorithm

John Daugman's algorithm uses an integro-differential operator to approximate inner and outer boundaries of the iris. It can also be used to detect the upper and lower eyelids by changing the countour integration from circular to arcuate [1]. The operator searches the image domain (x, y) for the maximum in the blurred partial derivative with respect to increasing radius r of the normalized contour integral of $I(x, y)$ along a circular arc ds of radius r and center coordinate (x_0, y_0) [1].

$$\max_{(r,x_0,y_0)} \left| G_\sigma(r) * \frac{\partial}{\partial r} \oint_{r,x_0,y_0} \frac{I(x,y)}{2\pi r} ds \right| \tag{1}$$

The Gaussian blur is given by $G_\sigma(r) = \exp(-r^2/\sigma^2)$.

2.3 Hough transform

Another method of iris segmentation highlighted in the academic literature is using a circular Hough transformation. The Hough transform is an algorithm presented by Paul Hough in 1962 for the detection of features of a particular shape like lines or circles in digitalized images [5]. The Hough transform is a widely used tool in image analysis for finding curves which can be defined in a parametrical form. The algorithm can be used to deduce the radius and placement of the pupil and iris regions [6].

The Hough transform has seen wide use in iris segmentation. Wildes [7], Kong and Zhang [8], Tisse et al.[9] and Ma et al. [10] have all used it for this purpose. Similar to Daugman's method, the Hough transform is also based on the first derivative of the image intensity. Wildes used the

method by first obtaining an edge map of the image by thresholding the magnitude of the image intensity gradient.

$$|\nabla G(x,y)I(x,y)| \tag{2}$$

Where $G(x,y)$ is a Gaussian smoothing function and the solution must obey the circle equation.

$$x_c^2 + y_c^2 = r_c^2 \tag{3}$$

2.4 Feature extraction using 2D Gabor wavelets

For feature extraction 2D, Gabor wavelets are commonly used, even in today's research. Daugman popularized the methodology in his initial paper, the methodology has since seen wide use in both commercial and academic applications.

Daugman used an encoding process illustrated in Figure 1. The central concept is a patch-wise phase quantization of the iris pattern. This is achieved by identifying in which quadrant of the complex plane each resultant phasor lies when a given area of the iris is projected onto complex-valued 2D Gabor wavelets, which are described by the following equation:

$$h_{\{Re,Im\}} = sgn_{\{Re,Im\}} \int_{\rho}\int_{\phi} I(\rho,\phi) e^{-i\omega(\theta_0-\phi)} e^{\frac{-(r_0-\rho)^2}{\alpha^2}} e^{\frac{-(\theta_0-\phi)^2}{\beta^2}} \rho d\rho d\phi \tag{4}$$

An interpretation of $h_{\{Re,Im\}}$ is as a complex-valued bit whose real and imaginary parts are either 1 or 0 (as a results of the *sgn* function). $I(\rho,\phi)$ is the raw iris image. α and β are the multiscale 2D wavelet size parameters, where Daugman's implementation chooses parameters such that they span an eight-fold range from 0.15 to 1.2 mm on the iris. 2ω is the wavelet frequency, being inverse proportional to β. (r_0,θ_0) are the polar coordinates in the region where the phasor coordinates are computed. In total, 2048 such phase bits are computed for each iris. This 256 byte sequence aims to uniquely identify a person [1].

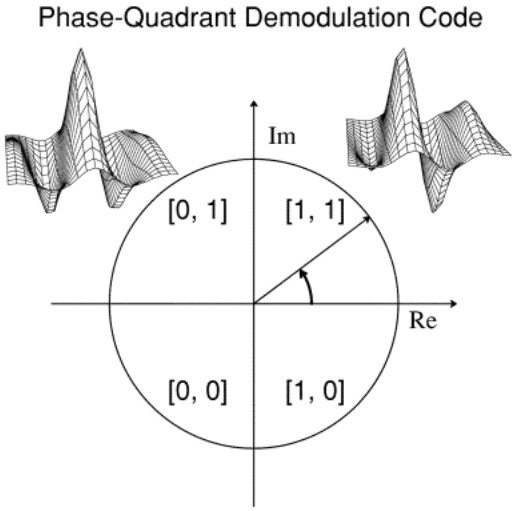

Figure 1: Phase demodulation process[1]

The phase demodulation process used to encode iris patterns is illustrated in Figure 1. Local regions of an iris are projected (2) onto quadrature 2D Gabor wavelets, generating complex-valued coefficients whose real and imaginary parts specify the coordinates of a phasor in the complex plane. The angle of each phasor is quantized to one of the four quadrants, setting two bits of phase information. This process is repeated all across the iris with many wavelet sizes, frequencies, and orientations to extract 2048 bits [1].

Since Daugman's initial proposal, variations of the method have been proposed (e.g [11]).

2.5 Fractional Hamming Distance

Daugman used the fractional Hamming distance as the measure of the dissimilarity between any two irises [1]. The respective phase code bit vectors are denoted as $\{codeA, codeB\}$ and the respective mask bit vectors as $\{maskA, maskB\}$. The mask bit vectors are set 0 where eyelashes are encoded and 1 for the iris, this makes sure that only the relevant bits are used for the distance metric. The fractional Hamming distance is then computed by the following equation:

$$HD = \frac{||(codeA \oplus codeB) \cap maskA \cap maskB||}{||maskA \cap maskB||} \tag{5}$$

The denominator keeps track of the total number of phase bits that were significant in iris comparison after artifacts such as eyelashes and reflections were discounted. The resulting Hamming distance is a fractional measure of dissimilarity. A perfect match is represented by a Hamming distance equal to 0.

2.6 Deep Learning for iris recognition

Other methodologies for iris segmentation and feature extraction have been exploited by researchers. In recent times, researches have proposed using machine learning for iris segmentation. In the beginning of 2019, a group of Chinese researchers achieved a 95.49% accuracy on the challenging CASIA-Iris-Thousand database using deep learning. The researchers used a combination of Faster R-CNN, Gaussian mixture models, and boundary point selection algorithms [12]. Similar methods have been used to better segment a wider range of images, providing more practical use [13].

3 Methodology

The methodology section considers the algorithms and procedures used in the implementation part of the project for iris delineation, feature extraction, and pattern matching.

3.1 Data description & source of data

The data used comes from the MMU Iris dataset [14]. The dataset contains 460 iris images of 46 persons. There are 5 images of both eyes for each person. All images in the dataset have been converted to grayscale. The dataset is freely provided by the MultiMedia University (MMU).

3.2 Stages of iris recognition algorithms

There are normally three stages for iris recognition systems:

1. Image preprocessing
2. Feature extraction
3. Pattern matching

The preprocessing stage aims to extract the useful iris region. This stage considers iris localization, normalization, and image enhancement. The purpose of localization is to detect the inner and outer boundaries of the iris, in order to isolate the iris region. Normalization converts the iris image from Cartesian coordinates to Polar coordinates. Image enhancement can potentially compensate for low contrast and non-uniform illumination caused by the position of the light source.

Feature extraction utilizes texture analysis methods to extract features from the normalized iris image. Feature extraction identifies the most distinct features that are later used for accurate identification purposes.

For the pattern matching part, the Hamming distance is calculated between all images (except for the image itself). Eye images belonging to the same individual are labeled as 'same' meanwhile images from other individuals are labeled as 'different'. These distances are plotted in form of a histogram, where the labels distinguish distances between the same individual and others. Ideally, there should be no overlap between the two distributions 'same' and 'different'. No overlap means that the algorithm can accurately classify the individual according to its eye image.

A visualization of the different steps can be seen in Figure 2 below:

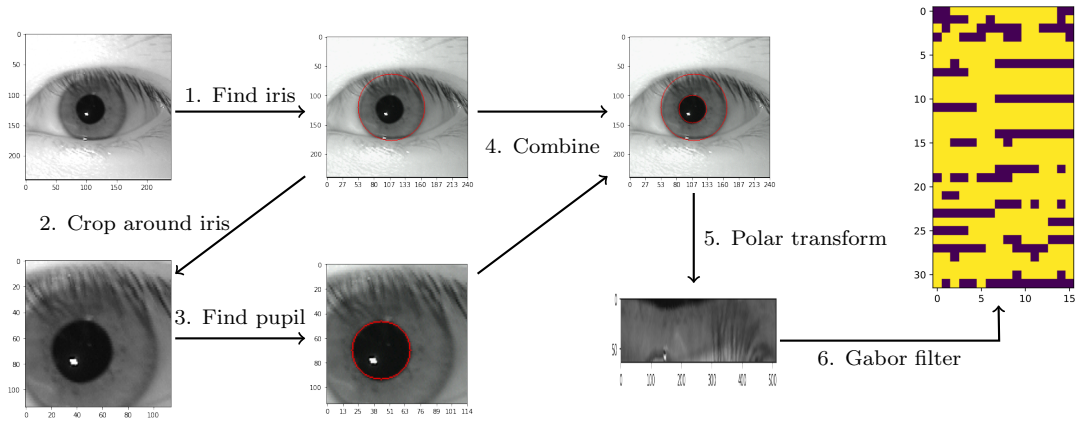

Figure 2: Iris localization and feature extraction procedure.

3.2.1 Cropping the image

The image is cropped in order to facilitate the iris segmentation and reduce the search area for Daugman's algorithm. All images are originally rectangular. The rectangular image is cropped to a squared image by decreasing the width equally on both sides, so that the width is equal to the height.

3.2.2 Gaussian blur

In order to reduce the noise of unwanted elements, for instance the hair from the eyelashes, Gaussian blur is used to smooth the image. The Gaussian filter used has a kernel size of $(15, 15)$, $\sigma_x = 5$ and $\sigma_y = 5$. Below is an illustration of what the filter does, after having cropped the original image.

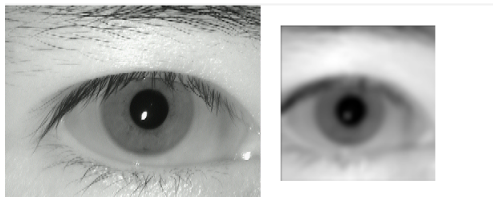

Figure 3: Original image (left), preprocessed image (right).

3.2.3 Iris localization

To locate the inner and outer boundaries of the iris, we use a discretized variant of Daugman's integro-differential operator as implemented in [15].

For the outer boundary of the iris, we limit the search for the iris center to the central 70% of both the x- and y-axis. If the input image is 100×100 pixels, the iris center is searched within $[15, 85] \times [15, 85]$.

Furthermore, a minimum and maximum radius of the shape allowed to be outlined is defined. For the outer boundary of the iris, the best results were obtained for a minimum radius of 45 and a maximum radius of 80.

To find the inner boundary of the iris (or the outer bound of the pupil), the search region is further narrowed proportional to the estimated radius of the iris. The image is cropped having a width and height of twice the iris radius, with the center of the image corresponding to the estimated iris center. For the inner boundary estimation, the scan ratio is reduced by 40% for both sides along both the x-axis and y-axis.

Below is an illustration of using Daugman's integro-differential opperator for finding the inner- and outer boundary of the iris.

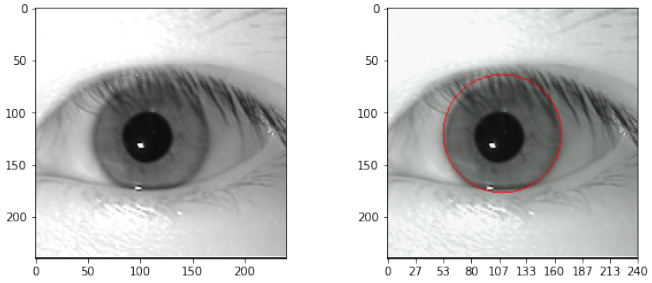

(a) Cropped image (b) Iris boundary outlined

Figure 4: Localization of the outer iris boundary with Daugman's algorithm

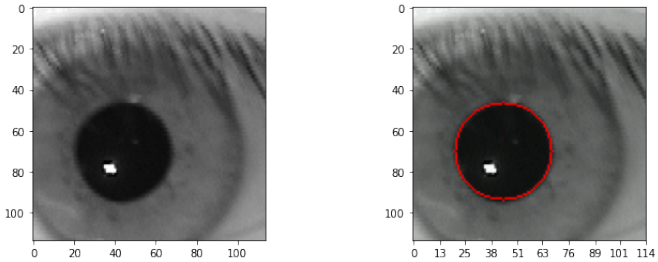

(a) Narrow search area, within the boundaries of the iris (b) Pupil boundary outlined by Daugman's method

Figure 5: Localization of the pupil boundary with Daugman's algorithm

3.3 Normalization

Images displaying irises may differ in size, position, the orientation of patterns, and illumination. Elastic deformations in the texture of the iris can affect the results. Thus, a representation that is invariant to the optical size of the iris, size of the pupil, location of the iris in the image, and the orientation must be used. This is achieved by using the same methodology as Daugman [1].

Each point on the iris, regardless of size and pupillary dilation, is assigned a pair of real coordinates (r, θ) where $r \in [0, 1]$ and $\theta \in [0, 2\pi]$. The mapping from raw cartesian coordinates (x,y) to this dimensionless nonconcentric polar coordinate system is described by:

$$I(x(r, \theta), y(r, \theta) \rightarrow I(r, \theta) \tag{6}$$

Where $x(r, \theta)$ and $y(r, \theta)$ are defined as:

$$x(r, \theta) = (1 - r)x_p(\theta) + rx_s(\theta) \tag{7}$$

$$y(r, \theta) = (1 - r)y_p(\theta) + ry_s(\theta) \tag{8}$$

The points $x(r, \theta)$ and $y(r, \theta)$ are linear combinations of both the set of pupillary boundary points and limbus boundary points along the outer perimeter of the iris [1]. The iris ring is anti-clockwised mapped to a rectangular block of fixed size (64 x 512). The remapping of the iris image $I(x, y)$ facilitates the extraction of features in the later stages of the iris algorithm.

Below is an illustration of how the iris looks like after this transformation to the polar coordinate system:

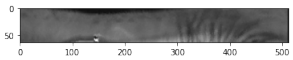

Figure 6: Normalization of the iris

3.3.1 Feature extraction

For encoding the iris features we use Daugman's [1] aforementioned classic 2D Gabor wavelet demodulation.

The report deviates from the exact methodology proposed by Daugman. Instead of applying multiple filters with a large range of parameters, we chose to use one filter with parameters proposed in similar work [16, 17]. Specifically, we use the Gabor filter defined as:

$$f(x, y) = \frac{1}{2\pi\sigma_x\sigma_y} \exp\left(i2\pi\omega\sqrt{x^2 + y^2}\right) \exp\left(-\frac{x^2}{2\sigma_x^2} - \frac{y^2}{2\sigma_y^2}\right) \tag{9}$$

with $\omega = 0.5$, $\sigma_x = 3$ and $\sigma_y = 1.5$. The filter is discretized by evaluating it at the points in the grid $[-9, -8, \ldots 8, 9] \times [-5, -4, \ldots, 4, 5]$, yielding a (19×11)-matrix. The normalized iris image is then convolved with the real and imaginary part of the discretized filter. The bit encodings are computed by splitting the convolved images into 8×8-submatrices and computing the sign of the sum of all elements in the submatrix. The real and imaginary bit encodings are in total 1024 bits.

Furthermore, the 1024 bit encoding is calculated multiple times for 7 linearly spaced rotations between $-\frac{\pi}{2}$ and $\frac{\pi}{2}$. This is to ensure that pattern matching can be done more efficiently, even for slightly rotated images.

The 2D Gabor Wavelet encoding is illustrated in Figure 7 below for two seperate images of three different individuals. As the encoding is binary, the plot displays a heat map over the grid of two colors. Note that we only display the encoding corresponding to the image convolved with the real filter. We can observe that the encodings are similar for the same individual but differs between individuals.

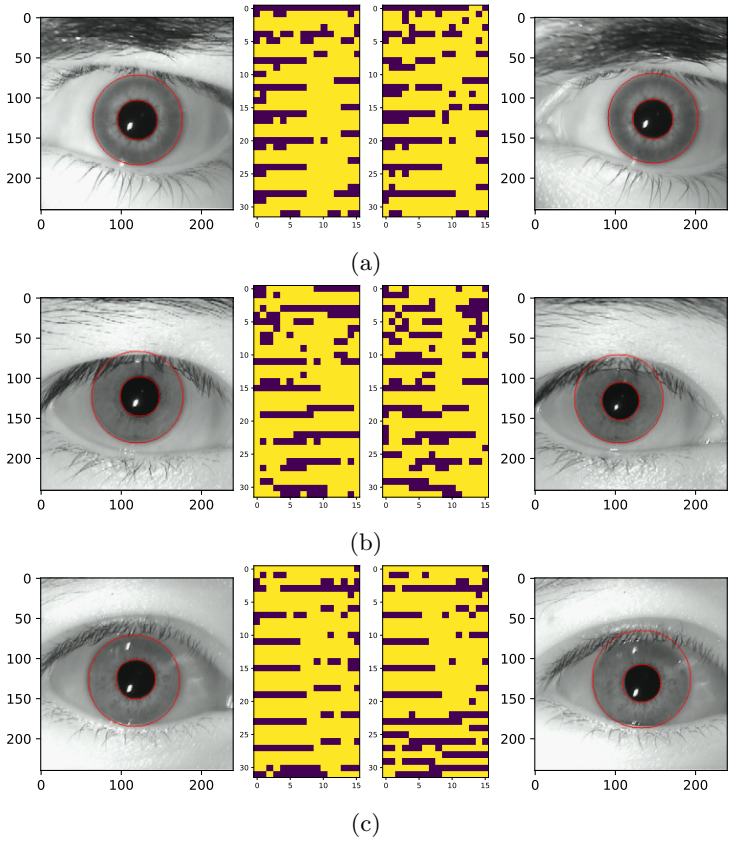

(a)

(b)

(c)

Figure 7: Comparison of extracted features in different images of the same eye. The real part of the extracted features $h_{Re,Im}$ are shown in the heatmaps.

3.3.2 Removal of inaccurate iris segmentation

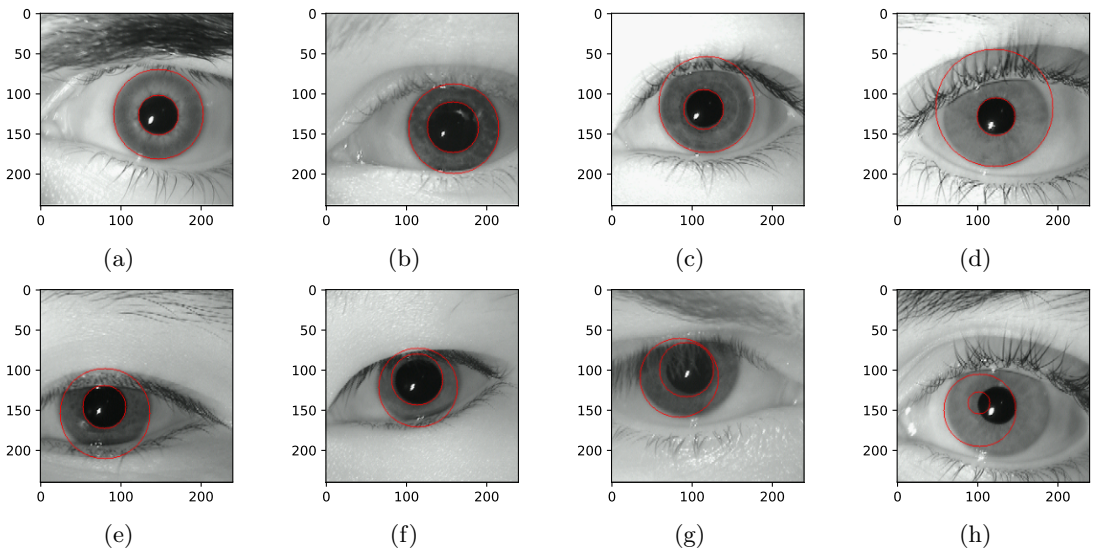

Figure 8: Examples of detected iris and pupil boundaries. In a), b) and c), the boundaries are ideal. In d), e) and f), the boundaries are decent but not ideal. In g) and h), the boundaries fail to capture a significant part of the iris and pupil.

For some images and individuals the integro-differential operator fails to find the inner and outer bound of the iris. Using these failed results will skew the results when doing pattern matching. Thus, these images are excluded from the pattern matching. Out of the 460 images, 340 images are classified as good (77.27%), 75 as bad (17.05%) and 25 as edge cases (5.68%). As edge cases yield adequate segmentation, these are included in the pattern matching. The classification is done manually.

An illustration of the detected boundaries is found in Figure 8. The figure displays the three different classifications as described in the figure text.

3.3.3 Pattern matching

In this report we deviate from Daugman's methodology in that the authors use the Hamming distance as the measure of dissimilarity, as opposed to the fractional Hamming distance. The Hamming distance between two vectors is given by the following equation:

$$HD = \frac{\sum(a \oplus b)}{n} \tag{10}$$

Where $\oplus$ is the 'XOR' operator and n is the dimensionality of the vector.

The Hamming distance is calculated between the input image and all other images (including rotated), classifying the image according to the shortest Hamming distance. Where the right and left eye are counted as separate classes, as they appear to have dissimilar iris patterns.

To assess the quality of our classification, we use the metric accuracy which is defined as the fraction of correctly classified datapoints out of all the classified datapoints.

To understand the effect of having multiple ground-truth images, we compare the accuracy when using 4 samples and 1 sample. When using 4 samples, we simply compare each image against the rest of the dataset - including 4 other images of the same person and eye. When using 1 sample, we randomly set aside 1 image per person and eye as the ground truth. The remaining images were then compared to the ground truth and classified to the closest image. This was repeated 30 times, the mean and standard deviation is reported in the results in Table 1.

4 Results

4.1 Distribution of Hamming distances

In Figure 9, the distribution of Hamming distances both between the bit encoding vector for different individuals and pictures of the same individual are illustrated.

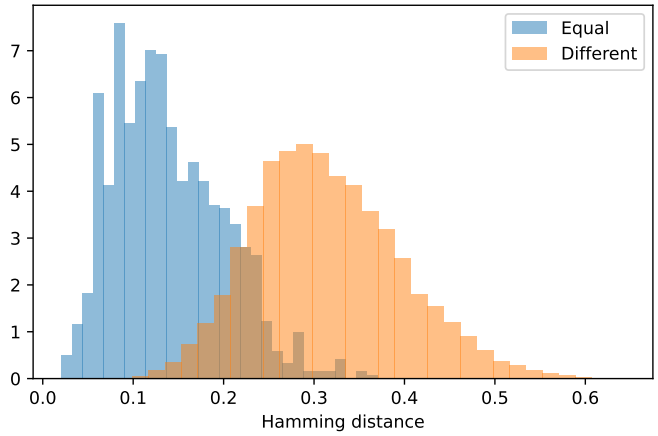

Figure 9: Distributions of Hamming distances. 'Equal' denotes the distances between images of the same individual whilst 'Different' denotes the rest. The left and right eye of the same individual are treated as different.

The results indicate that there is a distinct difference between the two cases, where the Hamming distance for the same individual is generally of less magnitude than the distance between individuals. However, the mean of the Hamming distance between individuals is not 0.5, as Daugman indicated ought to be the case for a good feature encoding [1], but around 0.3.

The overlap between the Hamming distances complicates classification. However, as we will see in the next section, the results are accurate non-the less.

4.2 Accuracy

In Table 1, the accuracy of the classification is displayed. The samples indicate the number of pictures used as data to make a prediction, as expected the accuracy declines when the model is given less data.

4 samples	1 sample
95.8%	$77.7\% \pm 2.4\%$

Table 1: Accuracy of iris classification.

5 Conclusions and research implications

The report shows that while using simple means, the information contained in the iris is a strong way to identify a person. Full-scale iris recognition can be implemented with a relatively low computational complexity, while yielding accurate results.

The procedure can be used in a number of commercial applications to enable secure authentication, as illustrated by the commercial adoption following Daugman's findings.

Branching outside of identification, Daugman's integro-differential operator could be used for a multitude of applications in image analysis. E.g finding the outline of a person's head, finding the ball on a football pitch, outlining planetary boundaries and much more.

While John Daugman managed to fully commercialize a methodology much akin to what this report uses, the field is rich in new research. Some areas where this report leaves room for further research is:

1. To use an increased number of 2D Gabor Wavelet filters with a systematic approach to parameter estimation
2. Applying Daugman's integro-differential operator once more, but changing the countour integration from circular to arcuate to identify the outline of the eyelids
3. Modifying the Hamming distance to neglect the bits encoding eyelashes
4. Enhancing the image after normalization to better highlight the iris' features (e.g using histogram equalization)
5. Comparing to different methods of iris segmentation (e.g Hough transform) and feature extraction/pattern matching (e.g Deep learning)

References

[1] John Daugman. "How Iris Recognition Works". In: *IEEE Transactions on Circuits and Systems for Video Technology* 14.1 (2004), pp. 21–30. DOI: 10.1109/tcsvt.2003.818350.

[2] Richard Ng, Yong Haur Tay, and Kai Mok. "A review of iris recognition algorithms". In: *Proceedings - International Symposium on Information Technology 2008, ITSim* 2 (Sept. 2008), pp. 1–7. DOI: 10.1109/ITSIM.2008.4631656.

[3] Stephen Mayhew. *Explainer: Iris Recognition*. 2012. URL: https://www.biometricupdate.com/201206/explainer-iris-recognition (visited on 04/21/2022).
[4] Alice Nithya and C. Lakshmi. "Iris recognition techniques: A Literature Survey". In: *International Journal of Applied Engineering Research* 10 (July 2015), pp. 32525–32546.
[5] Wojciech Wojcikiewicz. "Hough Transform, Line Detection in Robot Soccer". In: *Coursework for Image Processing* (2008).
[6] A. Bouridane. "Recent Advances in Iris Recognition: A Multiscale Approach". In: *Springer Science+Business Media* (2009).
[7] R. Wildes. "Iris recognition: an emerging biometric technology". In: *Proceedings of the IEEE* 85 (1997).
[8] W. Kong and D. Zhang. "Accurate iris segmentation based on novel reflection and eyelash detection model". In: *International Symposium on Intelligent Multi-media* (2001).
[9] C. Tisse et al. "Person identification technique using human iris recognition". In: *Proceedings of the Vision Interface* (2002).
[10] L. Ma, Y. Wang, and T. Tan. "Iris Recognition Using Circular Symmetric Filters". In: *National Laboratory of Pattern Recognition* (2002).
[11] Kshamaraj Gulmire and Sanjay Ganorkar. "Iris Recognition Using Gabor Wavelet". In: *International Journal of Engineering Research & Technology (IJERT)* 1 (2012).
[12] Li Yung-Hui, Huang Po-Jen, and Juan Yun. "An Efficient and Robust Iris Segmentation Algorithm Using Deep Learning". In: *Mobile Information Systems* 2019 (2019).
[13] Caiyong Wang et al. "Joint Iris Segmentation and Localization Using Deep Multi-task Learning Framework". In: *CoRR* abs/1901.11195 (2019). arXiv: 1901.11195. URL: http://arxiv.org/abs/1901.11195.
[14] Teo Chuan Chin. *MultiMedia University Iris database for Biometric Attendance system*. URL: https://www.kaggle.com/datasets/naureenmohammad/mmu-iris-dataset (visited on 04/20/2022).
[15] Borys Kabakov. *Daugman's algorithm for Iris detection*. 2021. URL: https://github.com/banderlog/daugman.
[16] Xiaodi Sun. *Iris Recognition*. 2018. URL: https://github.com/xs2315/iris_recognition.
[17] Akshata Patel, Hrishikesh Telang, and Aashna Kanuga. *Iris Recognition*. 2019. URL: https://github.com/akshatapatel/Iris-Recognition.